Improved Landing Radio Altimeter for Unmanned Aerial Vehicles based on an Antenna Array

Ronaldo S. Ferreira Júnior*, Marco A. M. Marinho*, Kefei Liu†, João Paulo C. L. da Costa*, Arthur V. Amaral* and Hing Cheung So†
*Department of Electrical Engineering, University of Brasília, Brasília, Distrito Federal, Brazil
†Department of Electronic Engineering, City University of Hong Kong, Kowloon, Hong Kong

***Abstract*—Unmanned aerial vehicles (UAVs) are used in various applications such as civil and military surveillance, law enforcement, and support in natural disasters as well as in hazardous environments. Approaching and landing are necessary steps for all UAVs, indicating that radio altimeters are needed. In this paper, a radio altimeter based on an antenna array is proposed. Our solution allows some improvements over the traditional radio altimeter such as more precise altitude estimation, ground imaging without the need of side looking radar, mapping the obstacles positions and detecting the ground inclination and topology. Another important contribution of this paper is a review of traditional radio altimeters along with a performance comparison between the level-crossing detection and the digital signal processing frequency detection - which is based on the fast Fourier transform algorithm.**

***Index Terms*—radio altimeter, unmanned aerial vehicles, antenna arrays**

I. Introduction

Unmanned aerial vehicles (UAVs) are used in various applications, such as civil and military surveillance, law enforcement, natural disaster situations, hazardous environments. Since UAVs are unmanned, they avoid the human risk and they are cheaper.

In large commercial [1] and military manned airplanes a radio altimeter acts as an auxiliary of the barometric altimeter and aids the landing and approaching. The altitude is measured based on the radar principle, with the target being the ground. However, unlike a simple pulse radar, where the target distance is measured by the round-trip-time (RTT), the measurement is made by a frequency-modulated continuous-wave (FM-CW) radar, where the phase difference, caused by the RTT, between the transmitted and scattered waves are exploited [1]–[4].

Usually, airborne radio altimeters are designed as low-power, low-range FM-CW radars, which operate in the 4.3 GHz frequency band [1], [5], [6].

The signal bandwidth plays an important role in determining the resolution and accuracy of the altimeters. For example, an FM-CW radar with a +/-100 MHz frequency deviation provides about 0.75 meter of resolution in a level-crossing frequency detection mode [2].

Although a 0.75 meter resolution seems to be rough, this resolution is still capable of aiding an UAV in cruising, landing and approach, and consequently, avoiding a plane crash given its fast response and capability to detect an obstacle, unlike a barometric or GPS altimeter [1].

Antenna arrays have been applied to improve the attitude estimation of UAVs [7], [8]. Since the antenna arrays are already included in the communication system, no additional hardware is necessary.

In this paper, we propose the application of antenna arrays to improve the altitude estimation, obstacle detection, as well as the landing area topology mapping and ground inclination measurement. The remainder of this paper is divided into five sections. In Section II the operational principle of the radio altimeter is introduced. In Section III, the traditional radio altimeter proposed by [1], [6] is briefly reviewed, and in Section IV, the proposed solution based on an antenna array is described. Simulation results are included in Section V to illustrate the traditional radio altimeter and the feasibility of the proposed solution. Conclusions are drawn in Section VI.

II. Operational principle of radio altimeters

Based on [1], a simplified FM-CW radio altimeter design block diagram is presented in Figure 1. A classic FM-CW radar uses a symmetrical triangular or saw-tooth wave as the modulating signal [2]–[4]. By using a symmetrical triangular waveform, the Doppler shift caused by the vertical speed or some other phenomena is canceled out [1], [3].

Typical frequencies for the modulating signal falls between 50 Hz and 300 Hz. If frequencies are below this range, the Doppler shift can cause severe distortion. On the other hand, if the frequencies are above this range, the output signal bandwidth is going to be higher, meaning that more thermal noise and other noises are going to be present, causing signal-to-noise ratio (SNR) degradation [1].

978-1-4673-2015-3/12/$31.00 ©2012 IEEE

Usually radio altimeters operate in the 4.3 GHz frequency band [1], [5], with a +/-100 MHz frequency deviation [2]. Transmitting power ranges from 10 dBm to 27 dBm [1], and the antennas are designed with a directivity around 10 dBi, allowing a wider ground area coverage [1].

In this design, the transmitted signal is generated by a voltage-controlled oscillator (VCO) and it is coupled to the receiver block mixer, acting as the local oscillator (LO) signal. The scattered signal, received by the receiver block antenna, is mixed with the LO signal, creating an intermediate frequency (IF) signal and a higher frequency signal which is rejected by the IF low-pass filter. The IF signal is then amplified through a limiting amplifier and fed to a zero-crossing detector, which is going to generate pulses for a frequency counter, or digital signal processing device so that the altitude information or some sort of obstacle alarm is displayed [1].

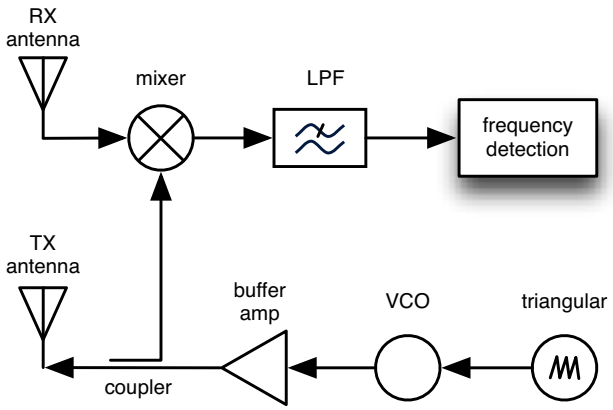

Figure 1. Simplified block diagram of radio altimeter [1].

III. Traditional Radio Altimeter

In this section, we present the mathematical model of a traditional radio altimeter by using communication concepts [3], [4], [9], [10].

The transmitted signal is frequency modulated using a VCO. A VCO is an electronic oscillator which changes its output signal frequency according to the input voltage, $v_{\text{in}}(t)$, weighted by a gain K_0 in [Hz/V] and $f_0(t)$ as the center frequency [11]:

$$f_{\text{VCO}}(t) = f_0 + K_0 \cdot v_{\text{in}}(t). \tag{1}$$

The instantaneous frequency of an FM signal is given by [10]

$$f_{\text{i}}(t) = f_{\text{c}} + k_{\text{f}} \cdot m(t), \tag{2}$$

where f_{c} is the carrier frequency, k_{f} is the gain and $m(t)$ is the modulating signal. Since the VCO output signal is closely realated to an FM signal, it is used to generate an FM signal [11].

At the VCO input, a triangle waveform $v_{\text{in}}(t)$ is used

$$v_{\text{in}}(t) = A_0 \cdot m_{\text{triangle}}(2\pi f_{\text{m}} t), \tag{3}$$

where A_0 and f are the amplitude and signal frequency, respectively. Considering that $f_{\text{m}} = \frac{1}{T}$, $m_{\text{triangle}}(2\pi f_{\text{m}} t)$ is a triangle waveform, which is a function of t, as illustrated in Figure 2.

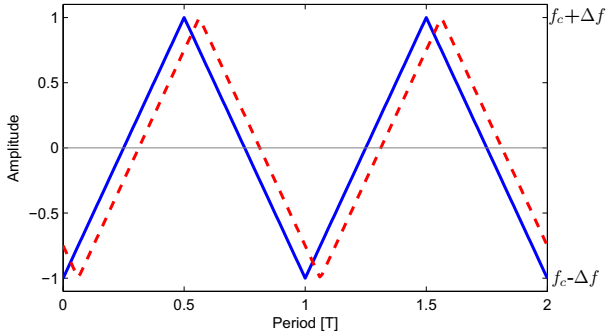

Figure 2. Modulating triangle waveform and its phase delayed version. At the positive or negative voltage peaks, the VCO outputs the center frequency, f_c, summed to the positive or negative Δf peak deviations.

The triangle wave is periodic. For one period, it is expressed as:

$$m_{\text{triangle}}(t) = \begin{cases} \frac{4t}{T} - 1 & \text{for} \quad 0 < t \leq \frac{T}{2} \\ \frac{-4t}{T} + 3 & \text{for} \quad \frac{T}{2} < t \end{cases}. \tag{4}$$

By combining (2) and (3), and considering $k_{\text{f}} \cdot A_0 = \Delta f$ (peak frequency devitation) [4], [10],

$$f_{\text{i}}(t) = f_{\text{c}} + \Delta f \cdot m_{\text{triangle}}(2\pi f_{\text{m}} t), \tag{5}$$

the phase term of an FM waveform is [10]

$$\xi(t) = 2\pi \int_0^t f_{\text{i}}(t')\,\mathrm{d}t' = 2\pi(f_{\text{c}} t + \Delta f \int_0^t m_{\text{triangle}}(t')\,\mathrm{d}t), \tag{6}$$

where $f_c = 4.3$ GHz is the carrier frequency, and $k_{\text{f}} \cdot A_0$ is chosen such that Δf = 100 MHz, providing a total frequency devitation of 200 MHz [1].

The VCO outputs a signal to be transmitted, $t_x(t)$:

$$t_x(t) = \cos\left[\xi(t)\right]. \tag{7}$$

When the signal is backscattered to the UAV, it suffers an amplitude attenuation, α and a time delay:

$$\tau = \frac{2r}{c}, \tag{8}$$

where c is the speed of light and r is the altitude.

The received signal is represented by:

$$r_x(t) = \alpha \cdot \cos\left[\xi(t-\tau)\right] = \alpha \cdot t_x(t-\tau), \tag{9}$$

The received signal is sent to a frequency mixer, after amplification by a factor of β, for frequency down-conversion.

The mixing with the local oscillator signal creates an IF signal, which is the so-called beating frequency signal:

$$\mathrm{IF}(t) = \beta\alpha \cdot r_x(t) \cdot t_x(t). \tag{10}$$

According to the trigonometric identities, the mixer output IF(t) contains the sum and difference of frequencies given by

$$\begin{aligned}\mathrm{IF}(t) = \frac{\beta\alpha}{2}\{&\cos\left[\xi(t) + \xi(t-\tau)\right] \\ &+ \cos\left[\xi(t) - \xi(t-\tau)\right]\},\end{aligned} \tag{11}$$

where the term with a high frequency component is suppressed by a low-pass filter located at the mixer output:

$$\mathrm{IF}'(t) = \frac{\beta\alpha}{2}\cos\left[\xi(t) - \xi(t-\tau)\right]. \tag{12}$$

The beating frequency from the filtered IF signal is:

$$\begin{aligned} f_{\mathrm{IF}'}(\tau) &= f_{\mathrm{i}}(t) - f_{\mathrm{i}}(t-\tau) \\ &= \Delta f \cdot [f_{\mathrm{c}} + \frac{4t}{T} - 1 - f_{\mathrm{c}} - \frac{4(t-\tau)}{T} + 1] \\ &= \Delta f \cdot (\frac{4\tau}{T}) \\ &= 4 \cdot \Delta f \cdot f_{\mathrm{m}} \cdot \tau. \end{aligned} \tag{13}$$

Since $\tau(r) = \frac{2r}{c}$, and (13) are linear, the output frequency is a linear function of either the time delay or the altitude. Moreover, the maximum altitude detectable should be less or equal to $\frac{1}{4}$ of $v_{\mathrm{in}}(t)$'s wavelength.

In (13), by substituting τ for (8), the detected frequency becomes a function of altitude [4]:

$$f_{\mathrm{altitude}}(r) = \frac{8 \cdot \Delta f \cdot f_{\mathrm{m}} \cdot r}{c}. \tag{14}$$

To make the design more compact, leaving space for more antennas, a single-antenna radio altimeter proposed by [12], would be very suitable for an UAV, due to its smaller dimensions and weight. The single antenna proposed in [12] is an FM radio altimeter system that is able to operate in continuous-wave (CW) and interrupted continuous-wave (ICW) modes, and uses a circulator as a duplexer, to separate the transmitted signal from the received signal.

IV. Proposed Radio Altimeter Based on Antenna Arrays

In this section, a novel radio altimeter is designed using an antenna array. A pulsed mode FM-CW radio altimeter is used, similar to the pulse compression radar (PCR) [2], operating in low pulse repetition frequency (PRF) mode.

By sending the signal in modulated pulses, the times of departure and of arrival are known, making the development of a direction of arrival (DOA) estimating radio altimeter possible, which is described in this section.

The antenna array radio altimeter is comprised of one transmitting antenna and a set of receiving antennas. Each receiving antenna has an individual receiving block, which contains the amplifying, mixing and filtering blocks.

It is important that each individual receiving block does not induce inter-element phase delays.

Figure 3 shows the backscattered wavefront impinging the antenna array, where θ is the actual wavefront DOA.

A. Data Model

The distance from the ground to the aircraft is far enough so that the wavefront is assumed to be planar.

According to the Carson's Rule [10], the bandwidth of the signal is relatively narrow in comparison to the carrier. Therefore, a linear mixture model can be considered to represent the received signal [13].

The output at the $m-th$ sensor, S_m, at the $n-th$ time instant is given by $x_m(n)$, containing d components related to the various scattering points on the ground. The signal is also added by an additive white Gaussian noise (AWGN), $n_m(n)$,

$$x_m(n) = \sum_{k=1}^{d} e^{-j.\mu(\theta_k).(m-1)} \cdot s_k(n) + n_m(n), \tag{15}$$

where the transmitted signal, scattered from the $k-th$ point on the ground, at the time instant n is represented by $s_k(n)$.

Let λ be the transmitted signal wavelength and Δ be the inter-element distance of the antenna array. The phase delay for the $k-th$ reflection impinging between two adjacent sensors is given by:

$$\mu(\theta_k) = \frac{2 \cdot \pi}{\lambda}\Delta \cdot \sin(\theta_k). \tag{16}$$

The entire system is written in matrix notation, yielding

$$\boldsymbol{X} = \boldsymbol{A} \cdot \boldsymbol{S} + \boldsymbol{N}, \tag{17}$$

The measurement matrix, $\boldsymbol{X}$, and the noise matrix, $\boldsymbol{N}$, are $M \times N$ matrices, where M is the number of antennas (length of antenna array) and N is the number of snapshots taken in time. The steering matrix, $\boldsymbol{A}$, and signal matrix, $\boldsymbol{S}$, have sizes of $M \times d$ and $d \times N$, respectively.

B. Direction of Arrival Estimation via Antenna Arrays

The DOAs of signals impinging over an antenna array can be estimated using a number of different algorithms. In this work, the estimation must be done with an estimator that offers good performance as well as

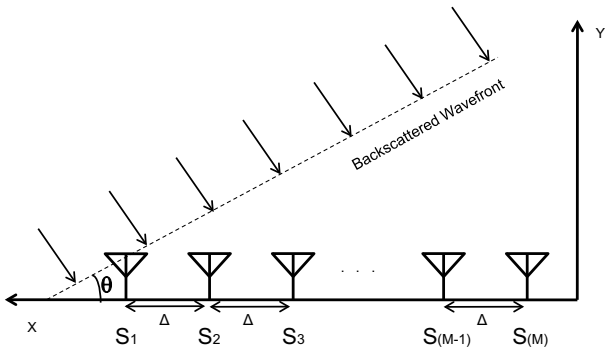

Figure 3. A wavefront impinging on an antenna array. The transmitted signal from the radio altimeter backscattered wavefront, impinging the antenna array.

computational efficiency. For this we turn to the subspace decomposition based DOA estimators such as MUSIC [14] and ESPRIT [15] which are the most popular and proven techniques.

The subspace methods are a direct application of principal component analysis (PCA), and rely on decomposing the received signal into two orthogonal subspaces, the signal and noise subspaces represented as Q_{s} and Q_{n}.

The Q_{s} contains the eigenvectors related to the signal and Q_{n} contains the eigenvectors related to the noise. However, the number of signals impinging over the array must be known *a priori* or must be accurately estimated using the model order estimation schemes, such as the Akaike information criterion [16]. The model order is represented here as d. Also, the distance between adjacent antennas in the array must not be larger than $\frac{\lambda}{2}$. Otherwise, the phase delay cannot be differentiated from its symmetric component over y in the unit circle.

In order to compute the signal subspace, we first define the covariance matrix of $\boldsymbol{X}$, which is given by

$$\hat{\boldsymbol{R}}_{\boldsymbol{XX}} = \frac{\mathbf{1}}{\boldsymbol{N}} \boldsymbol{X}\boldsymbol{X}^{\mathrm{H}}. \tag{18}$$

By using the covariance matrix, we can compute the signal subspace by applying the eigenvalue decomposition.

$$\hat{\boldsymbol{R}}_{\boldsymbol{XX}} = \boldsymbol{E}\boldsymbol{\Lambda}\boldsymbol{E}^{\mathrm{H}}, \tag{19}$$

where $\boldsymbol{\Lambda}$ is the diagonal eigenvalues matrix of $\hat{\boldsymbol{R}}_{\boldsymbol{XX}}$ and $\boldsymbol{E}$ is the eigenvector matrix, The signal subspace, Q_s is constructed using the eigenvectors related to d 's largest eingenvalues. The remaining eigenvectors form the noise subspace of Q_n.

A vector containing the relative phase differences between the signal measured at each component of the antenna array is expressed as

$$\mathbf{v}(\phi) = [1, e^{(-1i\cdot 2\cdot \pi\cdot d\cdot 1)\cdot \sin(\phi)}, e^{(-1i\cdot 2\cdot \pi\cdot d\cdot 2)\cdot \sin(\phi)}, \ldots \\ \ldots, e^{((-1i\cdot 2\cdot \pi\cdot d\cdot N-1)\cdot \sin(\phi)}]. \tag{20}$$

The MUSIC algorithm relies on the orthogonality of the signal and estimated noise subspaces. The MUSIC estimates the DOAs via maximizing the spectrum $M(\phi)$ which contains the estimated power of a signal arriving in a given ϕ direction:

$$M(\phi) = \frac{1}{\mathbf{v}(\phi)^{\mathrm{H}} \cdot Q_n \cdot Q_n^{\mathrm{H}} \cdot \mathbf{v}(\phi)}. \tag{21}$$

As ϕ becomes close to the DOA of a signal component the term $\mathbf{v}(\phi)^{\mathrm{H}} \cdot Q_n$ becomes increasingly small, the term does not reach zero due to inaccuracies in the estimation of Q_n, thus $\mathbf{v}(\phi)$ and Q_n are not completely orthogonal, but it still yields a large peak on the MUSIC spectrum. The d peaks of spectrum correspond to the estimated DOA of the d incoming waves over the antenna array.

The ESPRIT algorithm uses the signal subspace of Q_s to estimate the DOAs of the received signals. The ESPRIT relies on the fact is that the phase delay is the only difference between the impinging signals over two adjacent sensors in the antenna array. Given that the distance, Δ, between the two adjacent sensors is known, the phase difference has a direct relationship with the DOA. Let a selection matrix $\boldsymbol{J_1}$ selects the first $M-1$ rows of the subspace $\boldsymbol{A}$, and a selection matrix $\boldsymbol{J_2}$ selects the last $M-1$ rows of $\boldsymbol{A}$. Using the shift invariance equations, a $d \times d$ matrix, $\boldsymbol{\Phi}$, is obtained

$$\boldsymbol{J_1}\boldsymbol{A}\boldsymbol{\Phi} = \boldsymbol{J_2}\boldsymbol{A}, \tag{22}$$

in practice, one does not have knowledge of $\boldsymbol{A}$, but, since $\boldsymbol{A}$ and Q_s span the same subspace on the noiseless case, the DOAs can be estimated using the signal subspace

$$\boldsymbol{A} \approx Q_s\boldsymbol{T}, \tag{23}$$

where $\boldsymbol{T}$ is a nonsingular matrix that satisfies the given approximation, allowing $\boldsymbol{\Phi}$ to be obtained using Q_s

$$\boldsymbol{J_1}Q_s\boldsymbol{\Phi} = \boldsymbol{J_2}Q_s. \tag{24}$$

The d eigenvalues of $\boldsymbol{\Phi}$ contain inter-element phase delays for each of the arriving signals. They then map directly to the estimated DOA for each signal.

The ESPRIT method does not require peak searches, as the DOAs are obtained directly. But, on the other hand, the distance between each element of the antenna array must be constant and invariant. Errors in the positioning of the elements result in a large imprecision of the obtained DOAs estimation.

The MUSIC algorithm is well suited for arrays where precise positioning cannot be enforced. But this flexibility comes at the price of higher computational effort.

Given a proper estimation of the model order, the estimations are highly accurate and, as both methods depend on the subspace decomposition of the signal, the error of both algorithms is very similar. Both schemes are very robust to the presence of noise, given that the noise and signal components are decoupled in the subspace decomposition.

By estimating the DOA, a receiving lobe is simulated, as illustrated in Figure 4, raising the possibility to map the terrain and to monitor the topology of the eviroment around the aircraft.

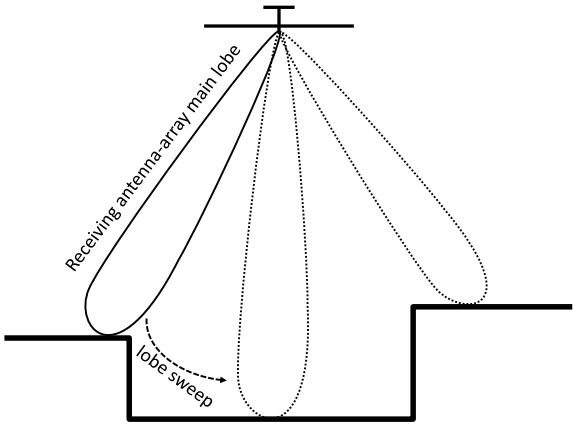

Figure 4. Receiving main lobe sweep for a M-antenna antenna array.

Since the lobe beamwidth decreases as the antenna array size increases [2], [3], [9], by using a large antenna array, higher mapping resolution is reached.

V. Simulation Results

The simulations contained in Figures 5 to 15 are based upon the diagrams shown in Figure 1.

The main simulations corresponding to Figure 3, are presented in Figures 12 and 14 and Figures 16 and 17, the other simulations in this Section are also valid, when considering an individual antenna from the antenna array.

The figures of merit evaluated include the altitude error for different SNRs

$$\mathrm{SNR}(r) = 10 \cdot \log_{10}\left(\frac{\sigma_s^2(r)}{\sigma_n^2}\right), \qquad (25)$$

where σ_s^2(r) is the signal variance at a given altitude, r, and σ_n^2 is the noise variance.

The signal-to-interference ratio (SIR), corresponding to the case when multipath signals are present, is

$$\mathrm{SIR} = 10 \cdot \log_{10}\left(\frac{\sigma_{\mathrm{LOS}}^2}{\sigma_{\mathrm{NLOS}}^2}\right), \qquad (26)$$

where σ_{LOS}^2 is line-of-sight (LOS) path signal variance, and σ_{NLOS}^2 is non-line-of-sight (NLOS) path signal variance.

In addition, the relation between the signal attenuation, the time (phase) delay and the altitude are also examined. Each result represents an average 100 Monte Carlo runs.

For simulation purposes, Δf=100 MHz, f_{m} = 300 Hz, so that, according to Equation (14), a variation of 1 meter corresponds to a frequency shift of 800 Hz.

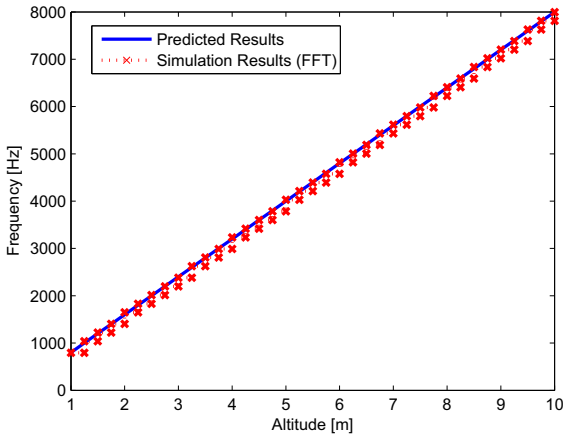

Figure 5. Frequency vs. altitude, for the predicted results, using Equation (14), and simulation results, using FFT. Time window = $\frac{1}{2}$ modulating frequency wavelength.

Figure 5 compares the empirical results using fast Fourier transform (FFT), to the predicted results in Equation (14).

The FFT is shown as a stair, due to its discrete nature. It has a significant goodness-of-fit with the predicted values.

The following 3 simulations present 5 cases, where different time windows were used to detect the signal. The time windows are measured in wavelengths of the modulating signal with a frequency of 300 Hz.

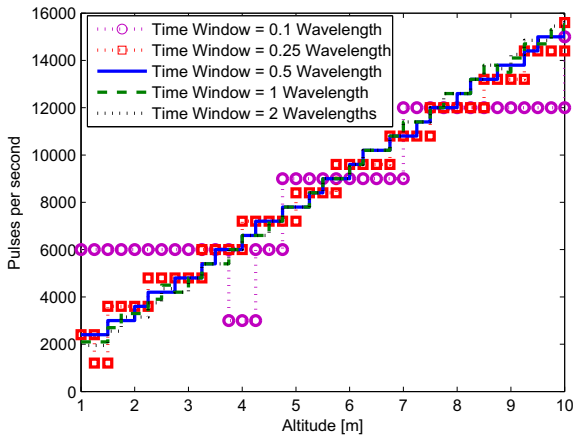

Figure 6. Frequency vs. altitude, simulated results for various time windows, level-crossing, no quadrature beat.

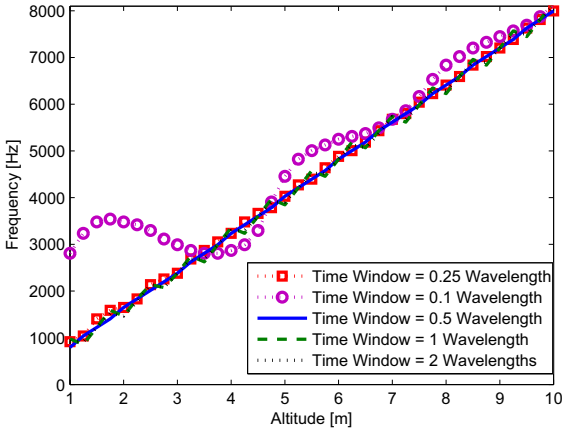

Figure 8. Frequency vs. altitude, simulated results for various time windows, FFT, no quadrature beat.

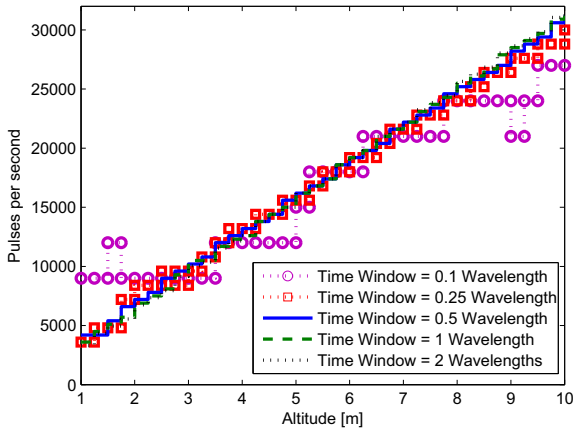

Figure 7. Frequency vs. altitude, simulated results for various time windows, level-crossing, with quadrature beat.

Figures 6 and 7 show how the level-crossing detector behaves using different time windows. Figure 7 shows the effect of a quadrature signal presence.

Both signals do not show satisfactory results with a $\frac{1}{10}$wavelength - time window, and the signal shows no significant improvement after using a $\frac{1}{2}$wavelength - time window.

Figure 8 depicts the behavior of the FFT detector for different altitudes. For the $\frac{1}{10}$wavelength - time window, there is a strong distortion, but for time windows of $\frac{1}{4}$wavelength and up the detection curve is satisfactory.

While satisfactory results with the quadrature receiver and level-crossing detection using a $\frac{1}{4}$wavelength - time window are achieved, similar results would be achieved with a non-quadrature receiver using a FFT detector. Hence, the complexity of the receiver is lowered, because less components are used, less power is spent, rendering into a smaller and lighter-weight apparatus.

Figure 9 shows that the 3 curves are overlapped, for linearity comparison purposes. The frequencies from the level-crossing detector signals are corrected to match the FFT signal.

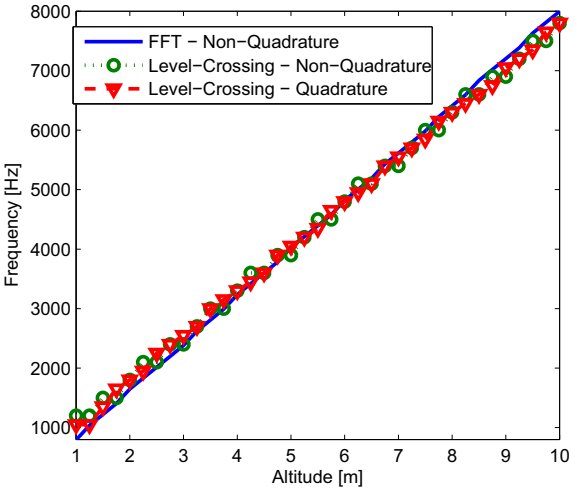

Figure 9. Frequency vs. altitude, detected frequencies from the 3 detection methods. The pulsed modes where weighted to match the FFT frequency. Time window = $\frac{1}{2}$wavelength.

Figure 10 shows the relative attenuation, obtained by the radar equation [2], [3], related to the altitude and time delay (τ).

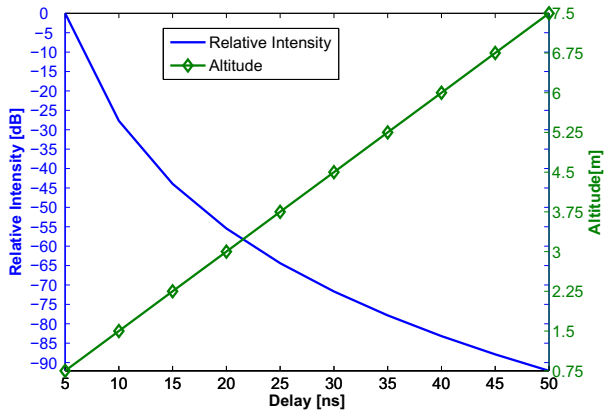

Figure 10. Altitude vs. delay vs. attenuation

The altitude estimation relative error versus SNR is shown in Figure 11, which indicates that the altitude estimation based on the FFT detector is more robust, achieving at least a 15 dB margin over the quadrature level-crossing detector.

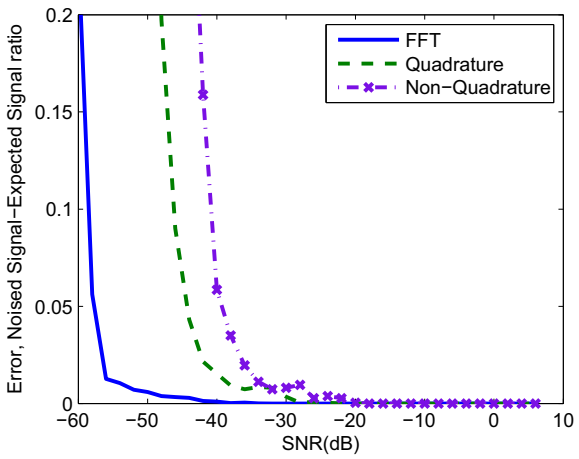

Figure 11. Relative altitude estimation error vs. SNR for quadrature and non-quadrature zero-crossing based radio altimeters [1] and the radio altimeter with FFT based frequency detection [6], altitude = 10 m, time window = $\frac{1}{2}$ wavelength.

In a real situation, the radio altimeter may receive the transmitted signal from various scattering sources and paths, thus the received signal is composed of the main signal and a number of multipath components that are scattered back to the antenna, generating interference. For analysis purposes the main signal path, which is perpendicular to the ground, called LOS path, and the other multipath components paths called NLOS paths, as illustrated in Figure 12.

For the altitude estimation, often, only the shortest path component is desired, because it represents the lowest altitude detected. Any other component that travelled a longer path should be considered as a form of interference.

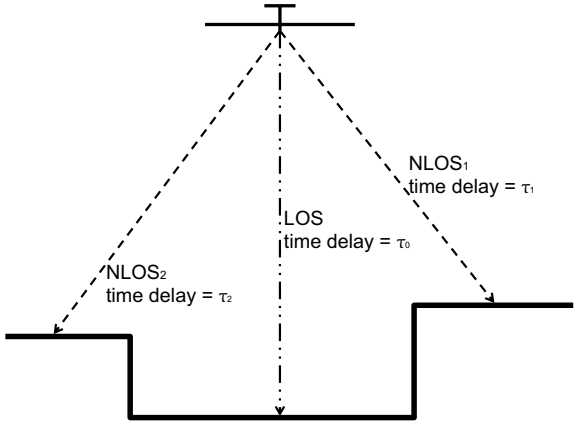

Figure 12. Line-of-Sight and Non-Line-of-Sight paths

Figure 13 illustrates the estimated altitude error caused by the SIR, evaluating how much a multipath component affects the overall performance. Two multipaths are assumed: one is the desired component, and the other is a multipath component that acts as the interference.

As Figure 13 shows, the altitude estimation relative error decreases as SIR increases.

When the interfering signal is getting the same power as the desired signal (near 0 dB SIR), the altitude associated with the interfering signal is detected instead, due the signal overlapping.

The interfering signal overlapping should not be considered as an undesirable effect every time. Since there is a high probability that if a NLOS path signal has a higher power than the LOS path signal, then the NLOS path signal was scattered back from an obstacle that is nearer to the UAV than the ground.

By observing Figure 12, the $NLOS_1$ is the shortest path, suffering less attenuation, that will be detected as the current altitude by the traditional radio altimeter. The spectrum of the received signal is shown in Figure 14.

There are other situations where a NLOS path signal could overlap the LOS path signal. For example, if the NLOS path signal reflecting surface, or obstacle, has a scattering coefficient or radar cross-section that is more advantageous than the LOS target, causing a high-power NLOS path signal reflection [6].

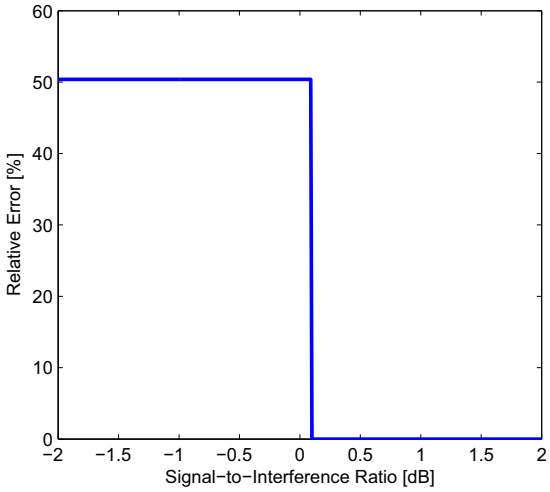

Figure 13. Signal-to-interference ratio (SIR) vs. relative altitude error. LOS path = 10 m, NLOS path = 15 m, FFT detection, time window = $\frac{1}{2}$wavelength.

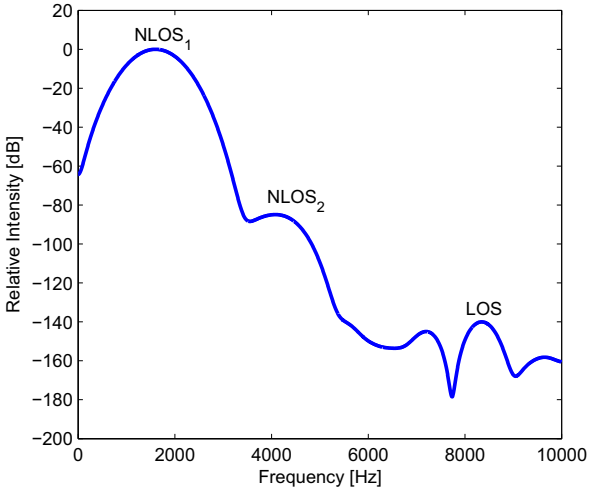

Figure 14. Spectrum of NLOS path signals linearly mixed with LOS path signal, based on Figure 12, where the $NLOS_1$ is the shortest path, FFT detection method, Chebyshev Window, time window = $\frac{1}{2}$wavelength, LOS path = 10 m, $NLOS_1$ = 2 m, $NLOS_2$ = 5 m.

Figure 15 evaluates the effect of a given LOS path signal mixed with a NLOS path signal, considering the path attenuation and high SNRs, over the detected frequency. For example, the dashed line with circles indicates a LOS path signal with the RTT = 5 ns, the detected frequency will remain fairly constant no matter which NLOS path signals, indicated by the horizontal axis, are mixed to it. Since the signals suffers attenuations higher than 10 dB/m, on plain ground surface the SIR is higher than 0 dB, so there are no signal overlappings.

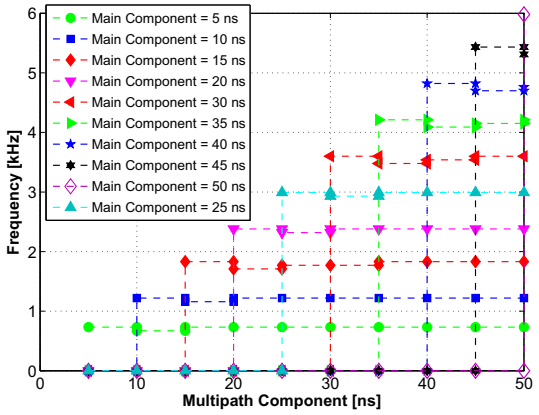

Figure 15. Delay vs. Frequency vs. LOS+NLOS, LOS path signal mixed with various NLOS path signals, FFT detection, time window = $\frac{1}{2}$wavelength.

However, in environments where a large number of NLOS path components are present such as an urban scenario, the altitude estimation suffers greatly from the interference, because the estimated altitude represents other obstacles than the ground itself.

Considering a situation as illustrated in Figure 14, the DOA estimation techniques, such as those presented in section IV, are needed, in order to achieve a correct altitude estimation.

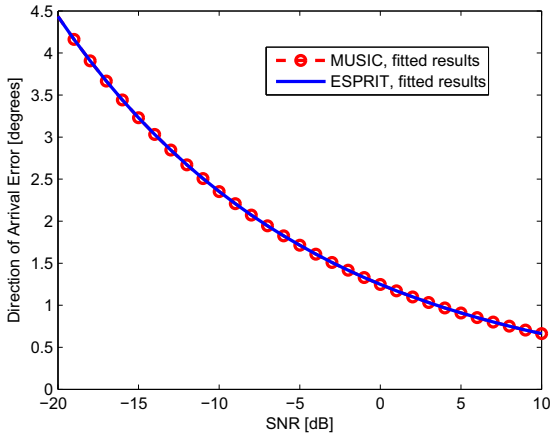

Figure 16. Direction of arrival estimation error vs. SNR, show in degrees the effect of the SNR on DOA estimation, for an antenna array of 2 receiving antennas.

Figure 16 illustrates the DOA estimation error versus SNR, when using a 2-antenna antenna array. In order to estimate the DOA accurately, the SNR must be high enough so that the DOA estimation error is kept low.

Figure 17 describes how the -4dB Beamwidth varies according to the number of antennas in the array, larger

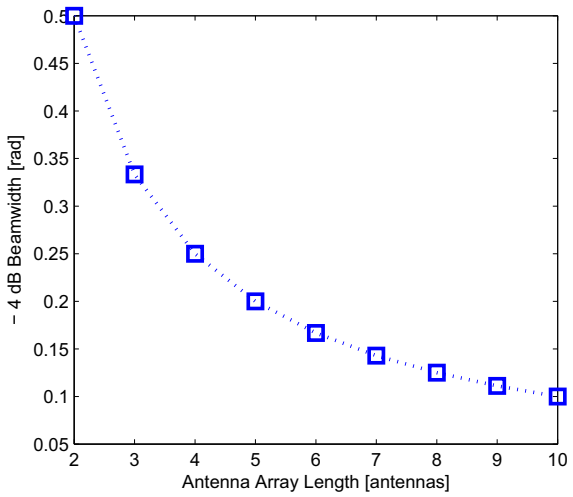

Figure 17. The -4 dB beamwidth vs. number of antennas in the antenna array, illustrates how the antenna array beamwidth, in radians, behaves as the antenna array increases its length.

the antenna array, narrower the beamwidth, thus, finer is the resolution. By using an antenna array, the spectrum in Figure 14, which is obtained from Figure 12, is solved. The LOS and NLOS path signals are separated by using a spatial component, the DOA, with a narrow enough beamwidth, so that the ground topology is mapped.

VI. Conclusions

In this paper, we have proposed an antenna array based radio altimeter. Our proposed solution allows to estimate not only the altitude, but also the inclination of the ground as well as possible obstacles and topology.

Besides the proposed solution, we also compare traditional radio altimeters based on level crossing and FFT detection. We show that the FFT allows a non-quadrature system, which has an improved performance compared to the level-crossing detector.

References

[1] Vidmar M., "A landing radio altimeter for small aircraft," in *12th International Power Electronics and Motion Control Conference (EPE-PEMC 2006)*, 2006, http://lea.hamradio.si/ s53mv/radalt/radalt.html.

[2] M. Skolnik, *Radar Handbook: Second Edition*, ISBN: 0071128026. McGraw-Hill, New York, 1991.

[3] G.W. Stimson, *Introduction to Airborne Radar*, Library of Congress: 8383041. Hughes Aircraft Company, El Segundo, California, 1983.

[4] Fred Nathanson E., *Radar Design Principles - Signal Processing and the Environment*, Library of Congress: 7980973. McGraw-Hill Book Company, New York, 1969.

[5] Werner Mansfeld, *Funkortungs- und Funknavigationsanlagen*, ISBN 3-7785-2202-7. Hüthig Buch Verlag GmbH, Heidelberg, 1994.

[6] Vidmar M., "Vertical navigation radar," 2008, http://www.s5tech.net/s53mv/vnr/design.html.

[7] J. P. C. L. da Costa, S. Schwarz, L. F. de A. Gadêlha, H. C. de Moura, G. A. Borges, and L. A. R. Pinheiro, *Attitude Determination for Unmanned Aerial Vehicles via an Antenna Array*, Proc. ITG IEEE Workshop on Smart Antennas (WSA'12), Dresden, Germany, March, 2012.

[8] K. Liu, J. P. C. L. da Costa, L. F. A. Gadêlha, H. C. So, and G. A. Borges, *Improved Attitude Determination for Unmanned Aerial Vehicles with a Cross-Shaped Antenna Array*, Proc. 14th IASTED International Conference on Signal and Image Processing, Honolulu, USA, August, 2012.

[9] M. Skolnik, *Radar Handbook: Third Edition*, ISBN: 0071485473. McGraw-Hill, New York, 2001.

[10] Simon Haykin, *Communication Systems: Fourth Edition*, ISBN: 0471178691. John Willey & Sons, Inc, New York, 2001.

[11] Roland E. Best, *Phase-Lock Loops*, ISBN: 0070050503. McGraw-Hill, New York, 1984.

[12] Leo G. Maloratsky, *An Aircraft Single-antenna FM Radio Altimeter*, May 2003.

[13] Andrea Goldsmith, *Wireless Communications*, ISBN: 9780521837163. Stanford University, California, 2005.

[14] R. O. Schmidt, *Multiple emitter location and signal parameter [J]*, 34:276-280. IEEE Trans on Antennas propagate, 1986.

[15] R. Roy and T. Kailath, *ESPRIT - Estimation of signal parameters via rotation invariance techniques*, IEEE Trans. Acoust., Speech, Signal Proc., vol. 17, no. 7, July 1989.

[16] Hirotugu Akaike, *A new look at the statistical model identification*, 716-723. DOI:10.1109/TAC.1974.1100705. MR 0423716. IEEE Transactions on Automatic Control 19 (6), 1974.